Bulletin of the Seismological Society of America, Vol. 92, No. 5, pp. 1766–1782, June 2002

Seismicity in Deep Gold Mines of South Africa: Implications for Tectonic Earthquakes

by Eliza Richardson and Thomas H. Jordan

Abstract We have studied induced seismicity associated with five deep gold mines located in the Far West Rand district, Republic of South Africa, focusing on the digital data recorded from January 1994 until February 2000 by in-mine arrays of three-component geophones. The observed seismicity, which exceeds 1,000 events per day, can be divided into two kinds of events, designated as Types A and B. Type A events are tightly clustered in time and space and generally occur within 100 m of an active mining face or development tunnel; their spectra are comparatively enriched in high frequencies, and they have an upper moment-magnitude cutoff at $M_{\max} < 1$. We associate these events with the "fracture-dominated" rupture of competent rock induced by dynamic stresses during blasting and quasi-static stress perturbations from the excavation and closure of individual stopes. In contrast, Type B events are temporally and spatially distributed throughout the active mining region; they represent "friction-dominated" slip in existing shear zones such as faults or dikes and have source-scaling properties that agree well with extrapolations from tectonic earthquakes. In the Far West Rand region, Type B events can have large magnitudes ($M > 3$), but they show a distinct lower magnitude cutoff at $M_{\min} \sim 0$. We interpret this cutoff in terms of a critical-patch size for nucleation of shear failure, and we show that the data are consistent with a rate- and state-dependent friction model in which the critical slip distance $D_c \sim 10^{-4}$ m. Both the spectral predictions of this model and accelerograms of Type B events agree that $f_{\max} \sim 200$ Hz.

Introduction

The physics of earthquake processes are most often studied at large scales through direct seismic observations or at small scales in experimental laboratory work. Seismic waves are usually recorded on regional seismometer networks located kilometers or more from the earthquake hypocenters, limiting the resolution of these data to scales of faulting that are typically greater than 100 m, corresponding to events with $M > 2$, in which M is moment magnitude as defined by Hanks and Kanamori (1979). Experiments under controlled laboratory conditions are feasible only on synthetic faults with dimensions less than about 1 m ($M < -2$). This results in an observational gap in the sampling of seismic processes that spans about 4 orders of magnitude in event size. Considerable progress has been made to shrink this gap by using local arrays, for example, Rubin *et al.* (1999), and instrumented boreholes, for example, Abercrombie (1995), Nadeau and Johnson (1998), Nadeau and McEvilly (1999), and Prejean and Ellsworth (2001). These studies incorporated seismicity down to $M \sim -1$ and have produced important results in extending and improving our knowledge of source scaling and fault behavior.

Such small-magnitude events are also of interest in the study of earthquake nucleation and the related phenomena of slip and stress heterogeneity on faults. The initiation of rapidly propagating shear ruptures on weak faults is thought to be governed by a critical slip distance D_c over which fault friction drops from a static to a dynamic value (Ida, 1972; Andrews, 1976a; Dieterich, 1986; Scholz, 1988). Constitutive rate- and state-dependent friction laws have been used to model laboratory data (Dieterich, 1979; Ruina, 1983); they yield estimates of D_c for bare surfaces on the order of 10^{-5} m (Marone and Kilgore, 1993; Marone, 1998). According to slip-weakening models, nucleation proceeds quasi-statically at an overstressed point on a fault until the slipping patch reaches a critical radius, when dynamic rupture will begin (Ida, 1973; Palmer and Rice, 1973; Andrews, 1976a; Dieterich, 1979). These models treat D_c as the nucleation distance over which slip is incurred on a finite-process zone ahead of a propagating crack tip, which for friction-dominated ruptures scales with the critical nucleation patch size r_c. This inner dynamic scale specifies a minimum earthquake magnitude $M_{\min}$. For example, a stress drop $\Delta\sigma = 0.3$ MPa, a shear modulus $G = 30$ GPa, and a $D_c = 10^{-5}$ m yield $r_c \sim (G/\Delta\sigma)\, D_c \sim 1$ m, corresponding

to $M_{\min} \sim -2.2$. Events of this magnitude are far below the detection thresholds of most surface seismometer and strainmeter networks.

It is not clear how best to extrapolate laboratory results to the scales of crustal faults. Large values of D_c (>10 cm) have been inferred from the high-frequency spectral cutoffs and barrier strengths observed for tectonic earthquakes (Ida, 1973; Aki, 1979; Papageorgiou and Aki, 1983a), which imply much higher minimum magnitudes: $M_{\min} > 2.5$ for stress drops less than 30 MPa. A possible explanation is that the effective critical-slip distance increases with fault-zone width W according to a strain-weakening model of the form $D_c = \gamma_c W$ (Andrews, 1976a; Aki, 1979). Laboratory data are consistent with a critical strain of $\gamma_c = 10^{-2}$, provided W is interpreted as the width of the fault zone actually participating in the slip, that is, the integrated shear-band thickness (Marone and Kilgore, 1993; Sammis and Steacy, 1994; Marone, 1998). The seismically derived values of D_c thus require wide (on the order of 1 m) shear-band thicknesses or additional mechanisms, such as near-fault damage, for energy dissipation at the rupture front. In the former case, the effects of the inner dynamic scale, including the lower magnitude cutoff, should be observable in the seismographic data. Aki (1987) presented evidence for a fall-off in seismicity below $M \sim 3$ from borehole-seismometer records in southern California, which he interpreted as support for a strain-weakening model with a large W. Studies of events in the Hokkaido corner and intermediate-focus earthquakes in Romania have shown similar seismicity fall-offs at $M < 3$ (Rydelek and Sacks, 1989; Taylor *et al.*, 1990; Trifu and Radulian, 1991). On the other hand, Abercrombie (1995) analyzed data from the deeper and more sensitive Cajon Pass borehole seismometers and detected no significant deviations from the Gutenberg–Richter frequency–magnitude relationship down to about $M = 1$ for southern California. Further studies of small earthquakes are necessary to understand the relationship among laboratory, local, regional, and global observations.

Mining-induced seismicity not only occurs at scales between those in the laboratory and those on tectonic faults but also can be recorded at the depth of seismic nucleation by using in-mine seismometers, thus creating an excellent "natural laboratory" in which to study the physics of earthquake rupture. Mine seismicity has been the subject of extensive investigation for nearly 40 years (Cook, 1963; Spottiswoode and McGarr, 1975; McGarr, 1984a; Gibowicz and Kijko, 1994). Much of this research has involved classification of these sources, and it is now widely accepted that there are two categories of seismic events: "those directly connected with mining operations . . . and those associated with movement on major geologic discontinuities" (Gibowicz and Kijko, 1994). While there has been much qualitative discussion about these two classes of events, relatively little quantitative investigation has been conducted to distinguish differences in their source properties. Some studies in Polish and Canadian mines have recognized that a break in the scaling relationship between number of events and energy occurs near $M = 3$ (Kijko *et al.*, 1987; Prugger and Gendzwill, 1990; Gibowicz and Kijko, 1994), but these studies were limited to seismicity of $M > 0$. Since the performance and sensitivity of the seismic networks have been greatly improved during the last 5 years by the installation of on-reef, three-component geophones, digital recording systems, and improved software for data processing (Mendecki, 1997), we have access to a wider range of event magnitudes that bridge the scale gap and enable detailed observations of the two classes of mining-induced events.

In this study, we have identified and described quantitatively two distinct populations of mining-induced seismic events recorded at five mines in the Far West Rand mining district in the Republic of South Africa (Fig. 1). We have developed a mechanical model to describe their differences and to relate these populations to the two classes that investigators have recognized previously. Events of the first kind, which we call Type A, are small ($M < 1$) and related directly to mining activity, whereas events of the second kind (Type

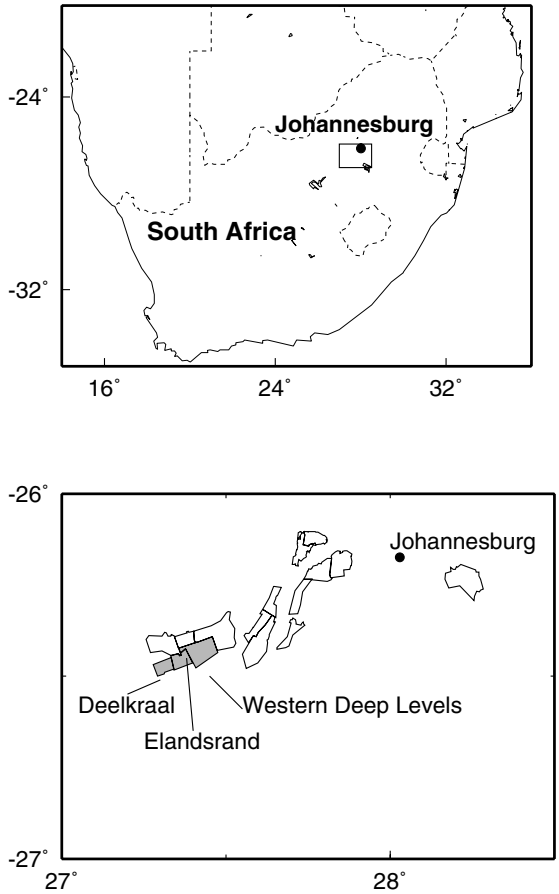

Figure 1. Southern Africa (top) and Far West Rand mining district, Republic of South Africa (bottom). The data in this study are from Deelkraal, Elandsrand, and the three Western Deep Levels mines (Mponeng, TauTona, and Savuka). Open outlines are lease areas of other mines in the region.

B) are larger ($M > 0$) and have source-scaling properties consistent with those of tectonic earthquakes. The lower- and upper-magnitude cutoffs observed for the Type B events define minimum and maximum scales of friction-dominated seismicity in this mining environment.

Seismicity Characteristics

The data in this study were recorded by on-reef networks of three-component, digital geophones operated by AngloGold, Ltd., and Integrated Seismic Systems, International, at five mines in the Far West Rand mining district, South Africa, approximately 80 km southwest of Johannesburg (Fig. 1). The five mines (Elandsrand, Deelkraal, Mponeng, Savuka, and TauTona) are the deepest in the world and extract ore from two gold-bearing quartzite reefs, the Ventersdorp Contact Reef and the deeper Carbon Leader Reef. These two units are separated vertically by 900 m, extend 2–4 km below surface in this region, and dip to the south at roughly 21°. The mines are very seismically active; the networks record ~1,500 events per day down to $M = -2$. Five months of seismicity at Mponeng include about 60,000 events (Fig. 2).

The data in this study were cataloged and processed by mine seismologists (see Table 1). We excluded from our dataset events recorded at fewer than four stations and events that appeared to be blasts that consisted of several small-amplitude, high-frequency arrivals spaced milliseconds apart. We included the hundreds of events triggered within seconds of daily blasting. Locations and magnitudes are well determined in the catalog; therefore, we have an extensive dataset for the analysis of frequency–magnitude statistics and spatio–temporal relationships of the seismicity.

The catalogs examined in this study comprise over half a million events (Table 1). For each of the five mines, we created frequency–magnitude distributions by binning the data in 0.1-moment-magnitude units and normalizing them to 30-day intervals to account for different catalog lengths (Fig. 3). The detection thresholds of the in-mine networks, as defined by the peaks of the discrete distributions, are all $M = -0.4$, except for Elandsrand, where it is $M = -0.2$. The seismicity rates fall off rapidly below these thresholds, except at TauTona, where the recent installation of a tightly spaced accelerometer array has increased network sensitivity in a small area (section 336 of TauTona). This is responsible for the higher cataloged rates observed for TauTona at $M < -1$ (Fig. 3a).

Above the detection threshold, the frequency–magnitude distributions share several characteristics that distinguish them from the Gutenberg–Richter (power-law) relationships often found for tectonic earthquakes. All show an initially rapid, though variable, rolloff just above the detection threshold, a sharp inflection to a much lower slope at about $M = 0$, a relatively narrow range of roughly self-similar behavior (b-value near unity), and then a concave-downward curvature up to a maximum magnitude of about $M = 3$. This shape appears to be caused by the superposition of two populations of events, which we label as Type A and Type B.

The largest event in this dataset has a moment magnitude of 3.3, but this upper cutoff is artificially limited by the catalog time spans. For example, events with $M > 3.5$ occur on an annual basis at Western Deep Levels, and mining-induced earthquakes have been recorded with moment magnitudes as high as 4 in the Far West Rand region. This upper-magnitude limit corresponds to a fault radius on the order of 1 km, which is intermediate to the lengths of the "long walls" commonly used in stoping (~200 m) and the lateral span of a whole mine (~3 km). Therefore, it likely reflects the regional extent of the stress perturbations associated with mining (McGarr, 1984b).

The Type A events form the maxima in the discrete distributions, accounting for the majority of the cataloged mine seismicity. The rapid rolloff from these peaks toward larger magnitudes indicates that the Type A events have an upper-magnitude cutoff near $M = 0$. The rolloff at low magnitudes reflects the detection threshold of the in-mine arrays, so that the scaling relationship for Type A seismicity cannot be inferred from the whole-mine catalogs used here. We note that previous work on very small events in situ, such as the study by Trifu *et al.* (1993) from Strathcona Mine, Ontario, Canada, found frequency–magnitude relations suggesting a departure from self-similar scaling due to enhanced seismicity in the range of $-0.5 < M < 0$, and their catalogs were complete to $M = -1.5$.

Differences in mining practices probably explain the differences in the distribution of events of $M < 0$ among the five mines. Most of these Type A events occur shortly after blasting, and their rates are therefore causally related to the amount of blasting, which varies from mine to mine. A detailed analysis of this relationship requires the consideration of two different Types of blasting: on the stope faces (for mining gold ore) and at the development ends (for extending tunnels, haulages, and spaces for other mine infrastructure). Such an analysis is not attempted here, although we note that the largest peak in the discrete frequency–magnitude distribution is observed for Mponeng, where the development rates are very high and some stope faces are blasted three times per day. Once per day is the norm for the other mines. The smallest seismicity peak is for Deelkraal, where the excavation rates are the lowest.

Despite the differences in mining practice and rates, the frequency–magnitude distributions for the events with $M > 1$ are similar among all five mines. The spatial and temporal distributions of $M > 1$ earthquakes are not directly correlated with day-to-day mining operations (compare Fig. 2a and 2b. From several lines of evidence discussed in the next section, we infer that this Type B seismicity is due to shear failures on zones of weakness and is therefore analogous to tectonic seismicity.

We performed a number of tests to determine whether the "bimodality" of the frequency–magnitude distributions

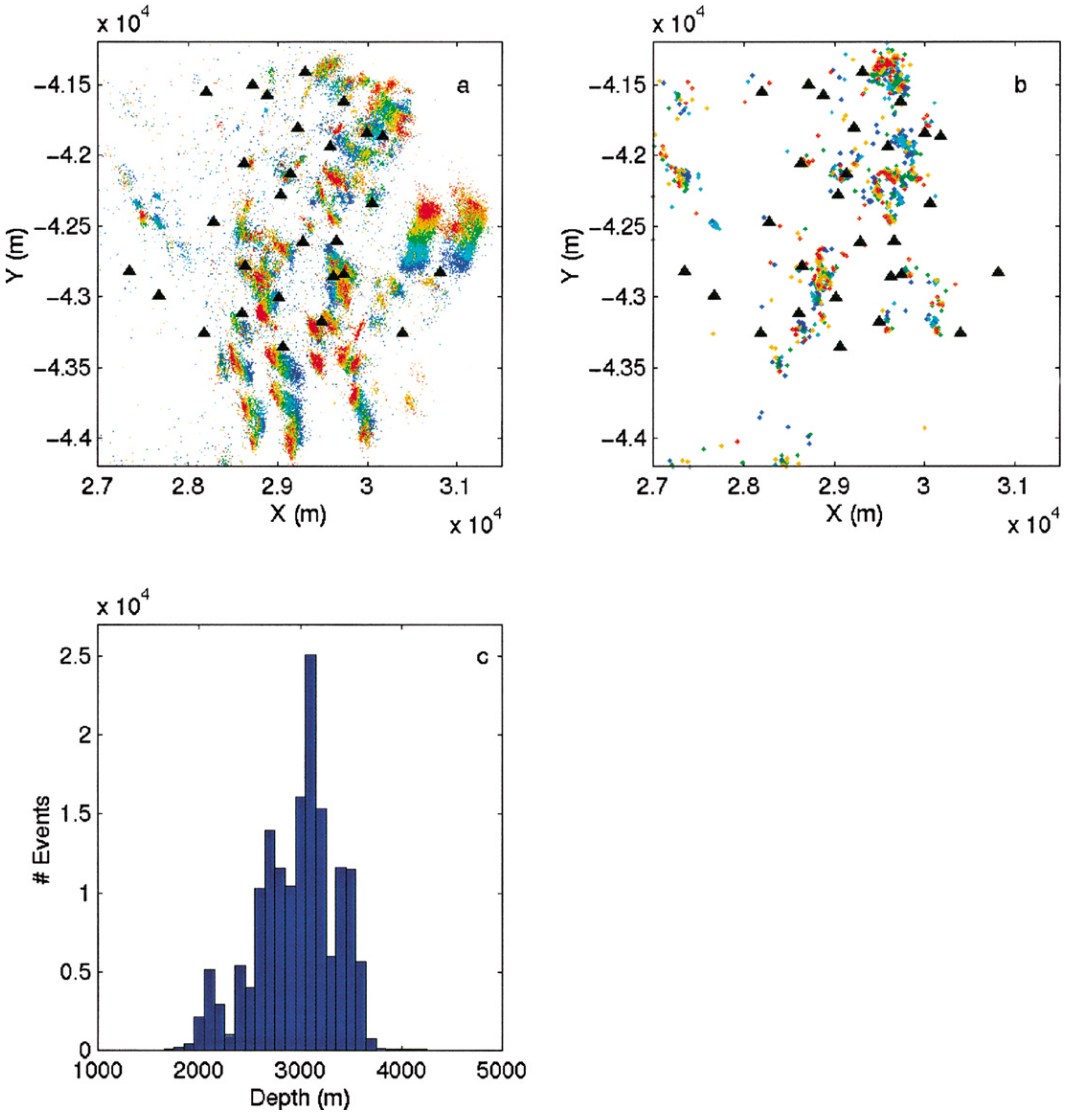

Figure 2. Map section in mine coordinates for a 5-month period (October–November 1998, January–March 1999) of all seismicity at Mponeng (a) and of $M > 1$ for the same catalog (b). Colors grade from cool to warm as the events become more recent, and triangles are geophone stations. The small events that dominate (a) track the progression of mining operations, while the large events in (b) are concentrated on weak geological features. Histogram of event depths for the three Western Deep Levels mines for the same time span (c).

Table 1
Mine Statistics

Mine	Catalog Span	Events	Stations	Reef
Mponeng	Oct–Nov 1998, Jan–Mar 1999	58,068	28	VCR
Savuka	Jan 1998–Mar 1999	54,125	23	VCR, CLR
Elandsrand	Jan 1994–Oct 1999	307,038	25	VCR
Deelkraal	Jan 1997–Oct 1999	70,240	13	VCR
TauTona	Jan 1998–Dec 1998	57,916	20	VCR, CLR

VCR, Ventersdorp Contact Reef; CLR, Carbon Leader Reef.

is an intrinsic property of the seismicity or whether it is an artifact of spatial sampling or another form of network bias that preferentially samples small events. For example, we compared the distribution in space of events in bins of 0.1-moment-magnitude units between $M = 0$ and $M = 1$ at Mponeng. No anomalous clustering of events was observed, and events of different magnitudes were found to be distributed equally throughout the coverage area of the seismic network. Even the smallest events are recorded across a distance covered by at least half of the array. Furthermore, when all events within 200 m of a station were eliminated from the dataset, the bimodal character of the distribution remained intact. The shape of the distribution also remained

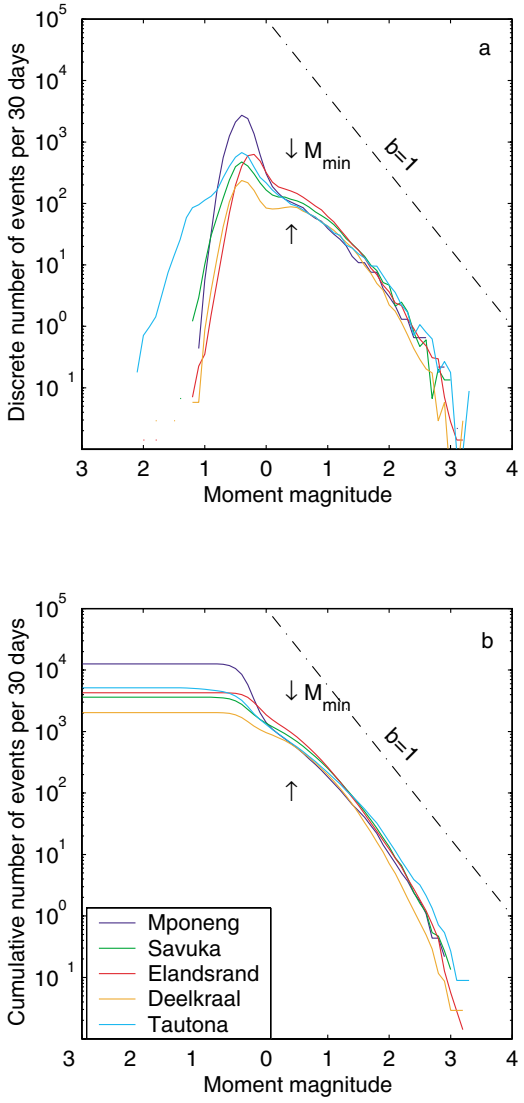

Figure 3. Discrete (a) and cumulative (b) Gutenberg–Richter distributions of seismicity per 30-day period in 0.1-magnitude-unit bins for Mponeng (blue), Savuka (green), Elandsrand (red), Deelkraal (orange), and TauTona (light blue). All mines have a bimodal frequency–magnitude distribution and are approximately alike above $M \sim 0.3$.

intact when the spatial extent of the dataset was successively reduced (Fig. 4). The top curve in Figure 4 is for a box 2.5 km on a side comprising almost 60,000 events from Mponeng, whereas the bottom curve includes only about 1,500 events from a 500-m box. The bimodality is preserved at all levels. This series of tests was repeated for the other four mines, with the same results.

These tests indicate that the unusual shape of the frequency–magnitude curves in the vicinity of $M = 0$ is not caused by network bias. In particular, the curvature observed for the Type B seismicity in the magnitude range $0 < M < 1$ appears to be a genuine feature of the distributions. Deelkraal shows a local maximum at $M = 0.4$, and the discrete distributions for the other mines are consistent with a Type B maximum at about this value, which we interpret as a lower-magnitude cutoff, M_{min}, for Type B events.

Comparison of frequency–magnitude distributions from time periods during which no blasting was conducted with distributions from time periods with regular blasting schedules confirms this interpretation (Fig. 5). The frequency–magnitude curve corresponding to the Christmas holiday when there was no blasting (black line) does not show the Type A peak that is apparent during normal mining operations (gray line).

The bimodal morphology apparent in Figure 3 has also been observed by Finnie (1999a,b). The existence of different classes of mining-induced seismicity has been noted previously by several workers (Kijko *et al.*, 1987; Johnston, 1988; Gibowicz, 1990; Johnston and Einstein 1990; Prugger and Gendzwill 1990; Gibowicz and Kijko, 1994; Finnie, 1999a,b), but only Finnie (1999b) successfully separated the two types spatially (he called them "genuine" and "spurious" events) and recombined them to produce a bimodal frequency–magnitude curve. The event populations that we define as Type A and Type B are likely similar to these two classes of events.

A Physical Model for Bimodal Seismicity

The attributes of Type A and Type B events suggest that they result from two fundamentally different processes of rock failure. Type A events are hypothesized to be fracture-dominated ruptures in a low normal-stress environment involving the failure of intact rock that responds at short time scales (seconds to minutes) to externally imposed stress changes such as blasting. Type A events may occur at scales as small as grain microcracks at the acoustic emission level up to scales limited by the stress-perturbation aureoles surrounding excavations. Because Type A events likely involve fresh cracking of rock that may result in little slip accumulation, their process zones are hypothesized to be smaller than the nucleation patch size expected for a slip-weakening model of shear strain (Barenblatt, 1959; Ida, 1972; Andrews, 1976a). Their radiated energy is high compared with that of Type B events that involve more slip.

Type B events are hypothesized to be friction-dominated ruptures that are also induced by mining but are the result of the removal of ore over a long period of time rather than to the most recent blasting activity. They entail slip on pre-existing planar zones of weakness, such as bedding planes, dikes, and reactivated faults. These weak zones do not necessarily have to be large, well-mapped features; they may be any surface upon which shear strain can easily be accommodated (Ortlepp, 1997), including old Type A fractures. We propose that the process zone of a Type B event is friction controlled, with a spatial size on the order of the critical patch size r_c, and is larger than that for a Type A event. Type B events may run away into the surrounding intact rock as they propagate, so that later excavation of their

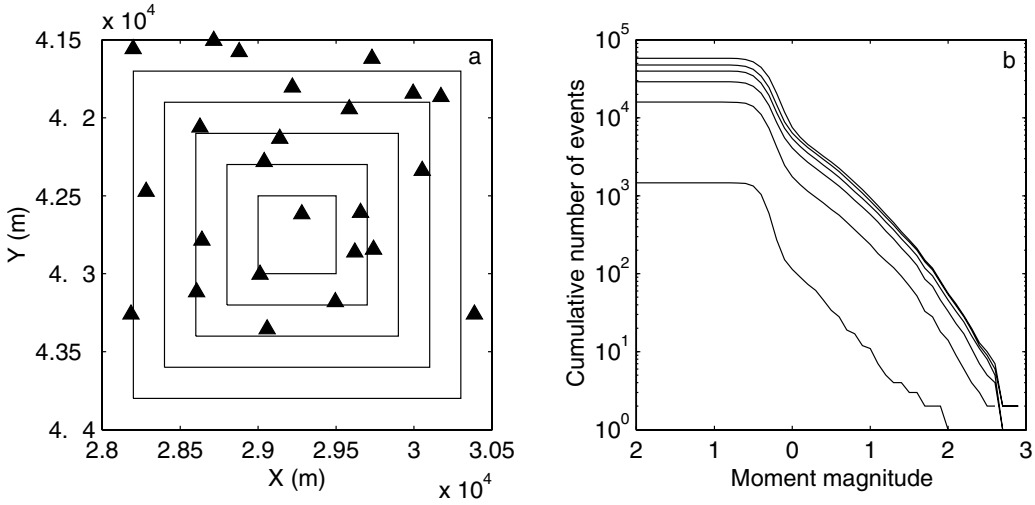

Figure 4. Plan view of Mponeng (a). Triangles are stations. Successively smaller boxes show the areas over which cumulative frequency–magnitude statistics in 0.1-M bins are calculated in (b). Largest box is 2.5 km on a side; box dimensions decrease by 200 m to inner box, which is 500 m on a side. In (b), the similarity in the cumulative distributions, which all show an inflection near $M = 0$, indicates that the shape is not biased by network sampling. We interpret the inflection to be the transition from Type A to Type B events.

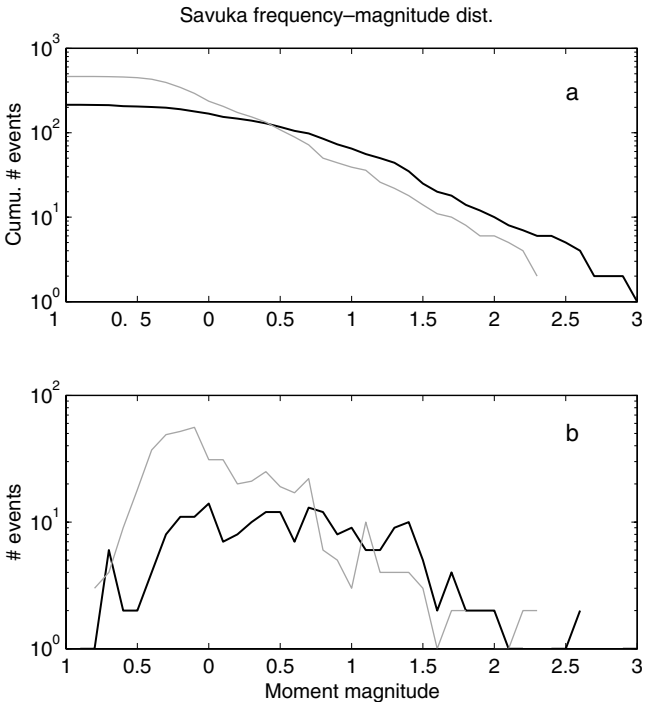

Figure 5. Cumulative (a) and discrete (b) frequency–magnitude distributions for Savuka for two 11-day periods. The grey line shows a regular blasting period, and the black line shows activity during the Christmas holiday when no blasting was conducted. Note the absence of the Type A peak during the Christmas holiday.

ruptures shows evidence of fresh fracturing, but their *initiation* is hypothesized to be controlled by the frictional properties of the process zone in which they nucleate. Owing to the similarity of their frequency–magnitude distributions among all five mines, we hypothesize that Type B seismicity is not affected significantly by different mining practices or rates.

Spatio–Temporal Relationships

Type A events occur as a series of distinctive swarms in space and time immediately following blasting and close to blasting sites. In this sense, they may be thought of as "aftershocks" of blasts. (Our knowledge of the response time of the Type A events relative to blasting is based on personal communication with the mine workers, since in general, blast times are not accurately recorded or documented.) In contrast, Type B events occur singly or, occasionally, as part of a foreshock-mainshock-aftershock sequence (Gibowicz 1997). They are distributed on structures throughout the entire mine instead of occurring only near active mining areas and can happen at any time of day. At Mponeng on 2 February 1999 between 1200 h and 1300 h, a Type B sequence occurred in the same time frame as several Type A clusters in different localities around the mine (Fig. 6). Shaded symbols show the Type B events. They comprise an $M = 3.0$ event, one foreshock, several aftershocks, and three events not related to that sequence. Mine workers have associated the sequence with a previously known mapped fault whose approximate location is shown by a dashed line (Fig. 6a). The sequence is linear in space, and its events do not cluster

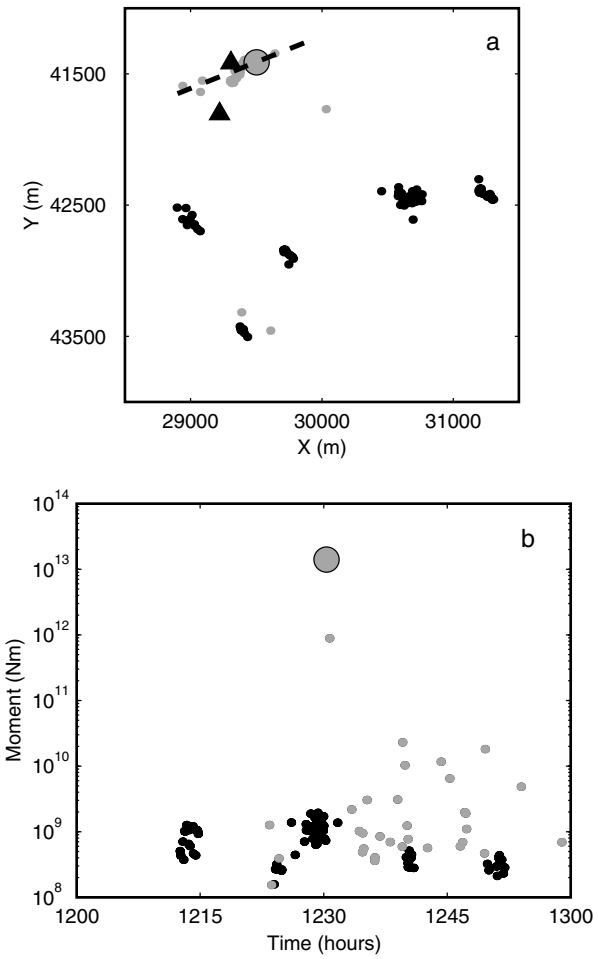

Figure 6. Map view of seismicity occurring between 1200h and 1300h in Mponeng, 2 February 1999 (a) and M_0 vs. time for the same events (b). Type A events are plotted as solid and Type B events as shaded symbols. In (a), triangles show two seismic stations, and the dashed line shows the approximate location of the normal fault thought to be associated with the Type B seismicity. The large shaded circle is an $M = 3.0$ event.

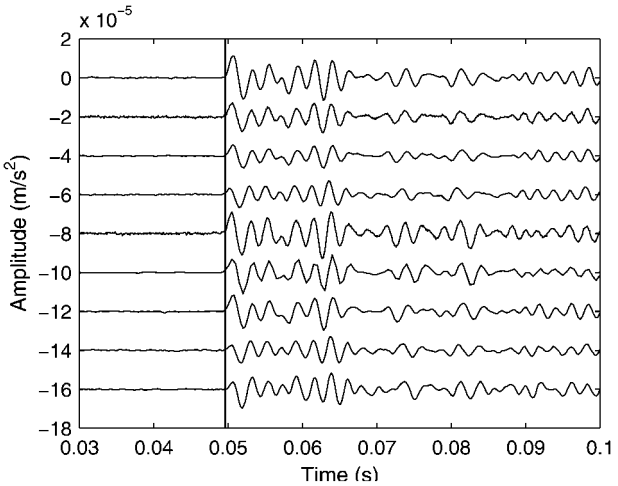

Figure 7. Waveforms of nine events in one of the Type A clusters in Figure 6 recorded at the same station. The actual values of the amplitudes are arbitrary, but scale is true. Each waveform has been offset from the others.

tightly in time, distinguishing them from Type A events. Black symbols show Type A clusters that are all associated with mine development (Fig. 6a). The same Type A events that make up each cluster in space are also clustered tightly in time (Fig. 6b). All of the Type A events are smaller than $M_0 \sim 2 \times 10^9$ Nm (Fig. 6b). We observe that Type A events of the same cluster have virtually identical waveforms; thus, they may represent successive failure of the same overstressed asperity or of the same propagating crack (Fig. 7).

The fact that Type A seismicity occurs in tight swarms in space and time allows us to separate the two types of events based on their clustering characteristics. We used an algorithm in which all events within a distance of 100 m and 30 sec of another event were classified as Type A, except for large ($M > 1$) events and their aftershocks. This separation technique excluded some Type A events that were missed by the chosen box size or time window, but it was designed merely to be a simple and quick way to define a large subset of events as clearly either A or B, so that the other differences in their properties could be studied. We tested the effectiveness of this algorithm with the 107 events in Figure 6. Initally, 37 events were classified as Type B and 70 as Type A. Based on waveform similarity, four events were reclassified as Type A. Of these, one had been missed because it fell outside the 30-sec time window, and the other three were slightly more than 100 m away from their nearest neighbors in the already defined Type A cluster to which they were reassigned.

The two types of events can be differentiated on the basis of visual inspection of their waveforms and spectra as well (Fig. 8). Type A events usually have lower *S*/*P* amplitude ratios than Type B events (Fig. 8a and 8c) and have a higher-frequency content (Fig. 8b and 8d).

Mechanisms

Much of the past study of event mechanisms in the mining environment has been limited by the quality of the available seismic data; therefore, many interpretations among previous workers have been inconsistent. Studies that analyzed *P*- and *S*-wave first motions interpreted fractures around stope faces as having isotropic components consistent with implosional mechanisms. These fractures were assumed to be related to closure of excavations and crushing of rock ahead of the stope face (Joughin and Jager, 1983; McGarr, 1992a). First-motion studies have also concluded that explosional isotropic events occur occasionally. However, all of these results have been debated because the coverage of the focal sphere often proved inadequate to reject a pure double-couple solution (Wong and McGarr, 1990). In addition, other first-motion studies and waveform analyses

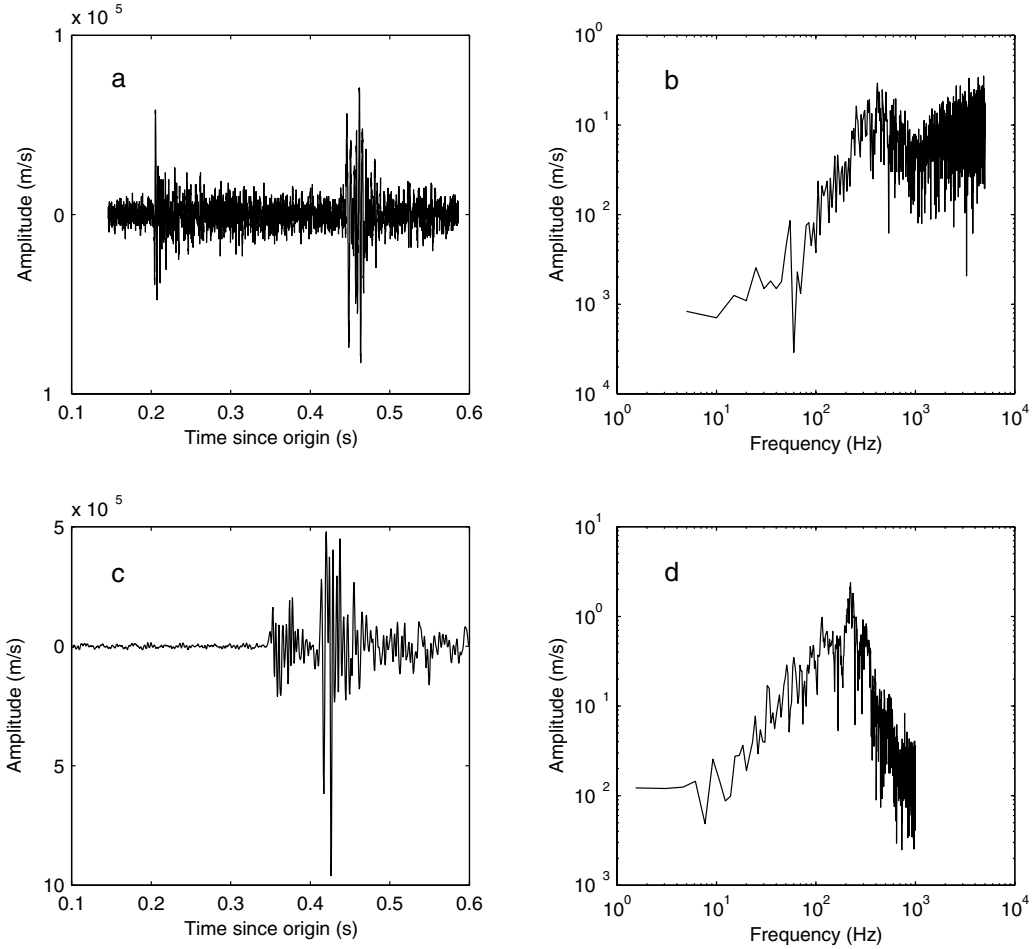

Figure 8. Vertical-component velocity seismograms for a Type A event (a) and a Type B event (c) recorded at Mponeng on 02 February 1999. In (a), the initial gap is the difference between the origin time of the event and the beginning of the triggered record. Each event's acceleration amplitude spectrum is shown to the right of the waveforms in (b) and (d). The Type A event is distinguished from the Type B event by its higher-frequency content and its lower *S*/*P* amplitude ratio.

found predominantly double-couple sources (McGarr, 1971; Spottiswoode and McGarr, 1975).

Recent developments using moment-tensor inversions to study focal mechanisms corroborate evidence that both pure double-couples and mechanisms with significant isotropic explosional components do exist (Talebi and Young, 1990; Feignier and Young, 1992; McGarr, 1992b; Baker and Young, 1997; Gibowicz, 1997; Andersen, 1999). In addition, studies of *S*/*P* amplitude ratios concluded that many of the $M < 0$ events had a significant tensile component (Cichowicz *et al.*, 1990; Gibowicz *et al.*, 1991). Our observations agree with these findings: Type A events have small *S*/*P* amplitude ratios compared with Type B events of approximately the same size (Fig. 8). This leads us to hypothesize that Type A events often have isotropic components, but Type B events are double-couple shear sources, consistent with our model of Type A events occurring in a low normal-stress environment that could induce mode I fractures, whereas Type B events occur in friction-dominated environments that induce planar shear ruptures.

Obtaining Source Parameters

Source properties of events in these catalogs are routinely determined at the mines via an automated spectral technique as outlined in Mendecki (1997). *P*- and *S*-wave displacement spectra are stacked and fit by the spectral shape (Aki, 1967; Brune, 1970)

$$\Omega(f) = \frac{\Omega_0}{1 + (f/f_0)^2} \tag{1}$$

in which Ω_0 is the long-period amplitude and f_0 is the corner frequency. These are the two independent parameters from

which seismic moment M_0 and radiated energy E are determined as follows (Mendecki, 1997):

$$M_0 = 4\pi\rho v^3 \Omega_0 \Re^{-1} \quad (2)$$

$$E = 8\pi^4 \rho \Omega_0^2 v f_0^3 \quad (3)$$

In these, ρ is rock density, v is the P- or S-wave speed, and $\Re$ is the root-mean-square radiation pattern, which is $\sqrt{4/15}$ for P waves and $\sqrt{2/5}$ for S waves. Source radius r, apparent stress σ_a, and static stress drop $\Delta\sigma$ are also determined by using $r = Cv/2\pi f_0$, $\sigma_a = GE/M_0$, and $\Delta\sigma = 7M_0/16r^3$, in which $G = \rho v_S^2$ is the shear modulus and C is a constant, chosen as 2.01 for P waves and 1.32 for S waves, after Madariaga (1976). Average values appropriate for this mining environment are ρ = 2,700 kg/m^3, v_P = 6,100 m/sec, and v_S = 3,650 m/sec. For a Brune spectrum, as in equation (1), σ_a and $\Delta\sigma$ are not independent (Andrews, 1986); therefore, using this technique to determine source parameters limits the investigation of source-scaling properties.

In addition, the processing routine used at the mines fixes the upper limit of f_0 at 300 Hz. This upper limit does not reflect bandwidth or sampling-rate limitations of the instruments; it is merely an artificial ceiling imposed on this source parameter. Therefore, many small events whose true corner frequencies are greater than 300 Hz are assigned a corner frequency at or just below 300 Hz by default. This in turn causes underestimation of E, σ_a, and $\Delta\sigma$ and overestimation of r.

Catalog Verification and Reprocessing

We reprocessed 228 events from Mponeng, Elandsrand, and TauTona in order to confirm the cataloged source parameters by using an independent method. In doing so, we followed Andrews (1986) and calculated displacement, velocity, and acceleration power spectra for every record of each event. We did not divide the velocity power spectra by 4 as in Andrews (1986), because this is a free-surface correction and the stations in this study are, at depth, embedded in the host rock. We median-stacked each event's spectra and integrated the results up to the value of the Nyquist frequency to determine $S_D{}^2$, the integral of the displacement power spectra (see equation 6 of Andrews [1986]), $S_V{}^2$, the integral of the velocity power spectra (see equation 7 of Andrews [1986]), and $\langle A^2 \rangle$, the acceleration power-spectral level (see equation 19 of Andrews [1986]). These are used to determine the following source parameters:

$$E = 4\pi\rho v S_{V^2} \quad (4)$$

$$M_0 = \frac{8\pi\rho v^3 S_{D^2}^{(3/4)}}{\Re S_{V^2}^{(1/4)}} \quad (5)$$

$$\Delta\sigma = \frac{2\pi\, f_0 \rho \langle A^2 \rangle}{C\Re}. \quad (6)$$

In equation (6), the corner frequency is found by $f_0 = (\sqrt{S_V{}^2/S_D{}^2})/2\pi$. Values of r and σ_a are calculated from E, M_0, and f_0 as in the previous section. This method has the advantage that $\Delta\sigma$ and σ_a are mathematically independent because the acceleration power-spectral level is used to find $\Delta\sigma$, therefore creating an extra degree of freedom in this calculation. Because our data are band limited, the energy we determined was less than the total energy radiated by the event (Ide and Beroza, 2001). However, in practice, the underestimation of energy for this dataset is very small, since our corner frequencies are generally 1/5 to 1/10 of the Nyquist frequency.

Our values of M_0 correlate well with those of the catalog, although the catalog value tends to be greater (Fig. 9a). The correlation coefficient is 0.94. Based on error analysis in which we assumed that the catalog error was some multiple of our error estimate, we found that the amount of scatter due to uncertainty was greater than the mean difference between our value and the catalog value. Both our measure and the catalog measure of M_0 have an estimated error of about 2%. Our measure of f_0 matches the catalog well for $1 \leq f_0 \leq 200$ Hz (Fig. 9b). The mean difference between the two measures is approximately 6 Hz, which is less than the expected uncertainty. For $f_0 > 200$ Hz, the discrepancies are much larger (mean difference is ~20 Hz). Except for two outliers, the catalog consistently underestimates f_0 of small events due to the 300-Hz ceiling (dashed line in Fig. 9b). The effect of the 300-Hz ceiling is not as sharply evident in Figure 9c because in the catalog, E is a nonlinear function of both f_0 and Ω_0 (see equation 3). Events with $E < 500$ J in the catalog are underestimated by the catalog because these correspond to the events whose corner frequencies are also underestimated. However, for $E > 500$ J, our values match the catalog values well within the expected uncertainty, which is ~10% for our estimate and ~12% for the catalog. The values of r that we determined correlate well with catalog values (correlation coefficient = 0.85) above $r \sim 10$ m. The scatter due to uncertainty is again greater than the mean difference between the two measures. Below $r \sim 10$ m, the catalog consistently overestimates r because of the 300-Hz ceiling in corner frequency. Overall, the catalog does a good job of determining source parameters for the Type B events. The accuracy of calculations for the Type A events suffers somewhat from the imposed restrictions on corner frequency that speed up the processing.

Source-Scaling Relationships

The two types of events have distinctly different energy–moment relationships (Fig. 10a). Energy increases with moment for the Type B events that we reprocessed. We do not have the bandwidth to assess the scaling of E with M_0 for the Type A events, although we observed that Type A events tended to have higher energies and therefore apparent stresses for the same moment as the Type B events. The apparent stress of Type B events increases with moment,

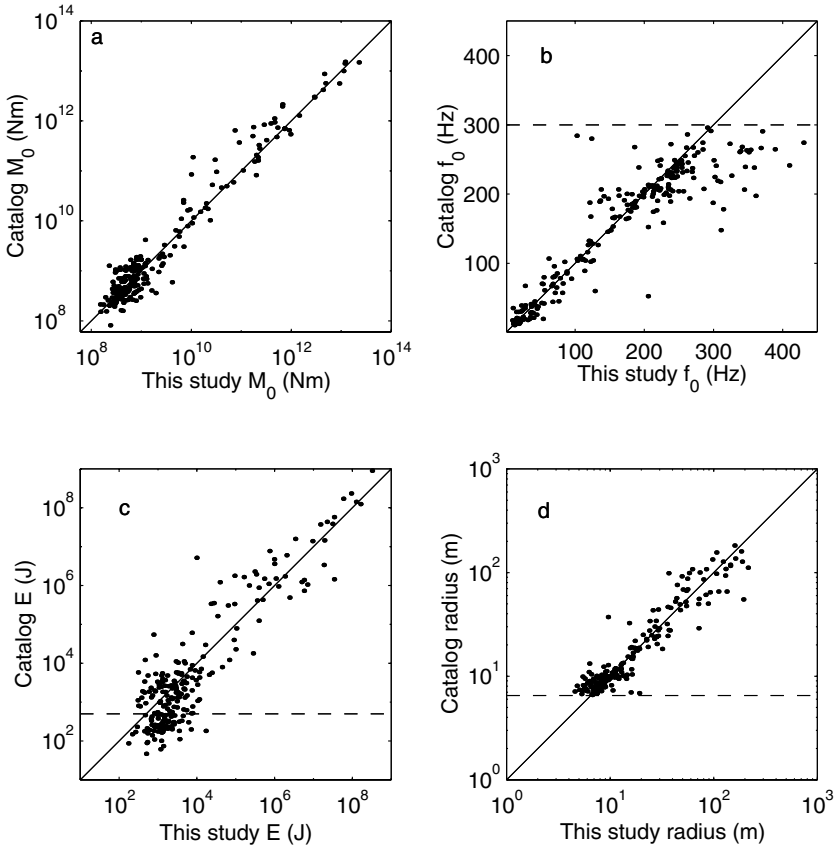

Figure 9. Comparison between our values determined by reprocessing and the values in the mine catalogs of M_0 (a), f_0 (b), E (c), and r (d) for 228 events in Mponeng, Elandsrand, and TauTona. Solid lines show 1:1 correspondence. Dashed lines in (b) and (d) show the the 300-Hz f_0 ceiling for the catalog data. Values below the dashed line in (c) are underestimated in the catalog due to the 300-Hz ceiling.

although there is much scatter (Fig. 10b). In this figure, plotted data points are the reprocessed events. The shaded line represents the median of the whole catalog (~450,000 events) binned in units of 0.1 order of magnitude in moment. At $M_0 < 3 \times 10^9$, the catalog data underestimate σ_a and $\Delta\sigma$, but for the Type B events, the catalog values correlate well with those that we determined in our subset of reprocessed data. A similar relationship of increasing $\Delta\sigma$ with M_0 is less visible (Fig. 10c); however, $\Delta\sigma$ and σ_a are well correlated (Fig. 10d), even though they are measured independently. The straight line in Figure 10d shows the exact relationship between $\Delta\sigma$ and σ_a for a Brune model shape (Andrews, 1986). The Type B events scatter about this line, but the Type A events are better described by a line with a shallower slope; that is, Type A events have a higher stress drop than a Brune model spectrum predicts. Given the correlation between $\Delta\sigma$ and σ_a, the Type B events appear to be have increasing $\Delta\sigma$ with M_0, just not as strong as the relationship between σ_a and M_0. It should be noted that these values of stress drop were calculated assuming constant rupture velocity, whereas the scaling of apparent stress with seismic moment indicates that rupture velocity may scale with moment. This analysis will be the subject of a subsequent study.

The Type A and B events in the Far West Rand region are distinguishable as separate populations and have characteristics consistent with our proposed model. Type A events are, on average, more energetic, with higher $\Delta\sigma$ and σ_a for a given moment, and are smaller events. They have scaling relationships that match well with other events that seem likely to represent fracture of competent, intact rock with small process zones. Type B events have scaling relations consistent with that of friction-dominated tectonic earthquakes, as our model predicts.

Implications of Type B Seismicity for Tectonic Earthquakes

Type B events appear to be analogous to tectonic earthquakes, based on evidence from their source-scaling properties, mechanism characteristics, and frequency–magnitude statistics. We now show that with reasonable assumptions about source-scaling relationships, we can use information from the inner scale of Type B seismicity to infer the critical patch size and slip distance for the minimum earthquake nucleating in this tectonic environment.

Estimate of Critical Slip Distance

Following Ida (1973), Dieterich (1979), and Aki (1987), we interpret the observed lower-magnitude cutoff for a Type B event in terms of a slip-weakening model that requires a minimum patch size with a critical slip distance for the nucleation of shear failure (see also Palmer and Rice, 1973; Andrews, 1976a,b; and Dieterich, 1986). Type B frequency–

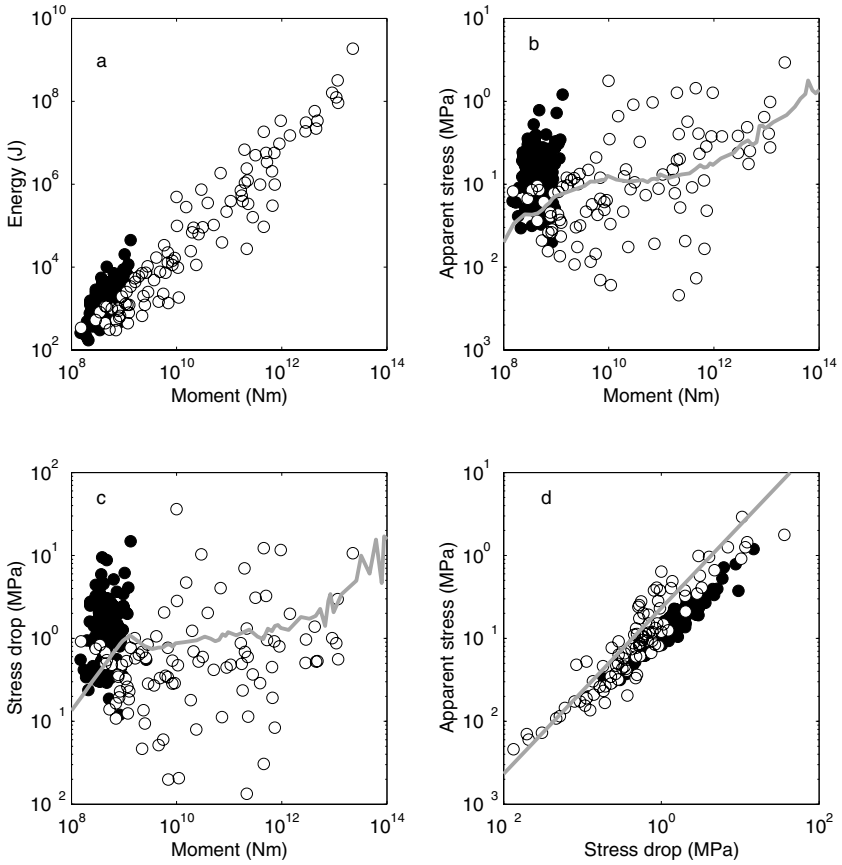

Figure 10. E vs. M_0 (a), σ_a vs. M_0 (b), $\Delta\sigma$ vs. M_0 (c), and σ_a vs. $\Delta\sigma$ (d) for the events we reprocessed. Type A events are plotted as solid and Type B events as open symbols. In (b) and (c), shaded lines represent the median values from the whole catalog (~450,000 events) binned in 0.1-order-of-magnitude units in moment. In (d), the straight line shows the exact relationship between σ_a and $\Delta\sigma$ for a spectrum with a Brune model shape.

magnitude distributions are alike among all of the mines and have consistent $M_{\min} \sim 0.4$ (Fig. 3). We take $M_{\min}$ as the local maximum in the discrete distributions, which is visible at Deelkraal and inferred for the other four mines by removing the Type A peak. We can then calculate the critical patch size r_c and the critical slip distance D_c for seismic nucleation by solving

$$r_c = \left(\frac{7M_0^{\min}}{16\Delta\sigma}\right)^{1/3} \tag{7}$$

and

$$D_c = \frac{16\Delta\sigma r_c}{7\pi G} \tag{8}$$

in which $M_0^{\min} = 4.7 \times 10^9$ Nm, the seismic moment corresponding to $M_{\min} \sim 0.4$, the static stress drop $\Delta\sigma = 0.3$ MPa, a good estimate of the average Type B stress drop in our datasets, and $G = 36$ GPa. We obtain $r_c = 19.0$ m and $D_c = 1.2 \times 10^{-4}$ m. This D_c is equivalent to the critical slip distance derived from standard rate- and state-dependent friction laws (Dieterich, 1978, 1979), assuming that $\Delta\sigma = \sigma_n (b - a)$, in which σ_n is normal stress and a and b are constants. Our calculation of D_c using these average values for the mining environment lies between representative results from laboratory data and tectonic earthquakes (Fig. 11). Uncertainties in D_c, shown by the size of the box in Figure 11, arise from several sources. Based on the range of values measured empirically for shear-wave speed and rock density, we expect the shear modulus G to have 5% uncertainty. The uncertainty in the average stress drop is about 50%, and the range of $M_{\min}$ has an uncertainty of about 25%. Thus, we expect an error of 20% in our estimation of r_c and 25% in D_c.

The D_c calculated here is considerably smaller than that determined by modelling large earthquakes (Scholz, 1988) but about an order of magnitude larger than values determined in laboratory experiments for bare surfaces or for thin gouge layers (Dieterich, 1979; Biegel *et al.*, 1989; Marone, 1998). If nucleation length scales by the strain across the active shear zone as in Marone and Kilgore (1993), mature faults with wide gouge zones require a larger effective D_c to nucleate seismic rupture than do bare surfaces. Shear zones in the mines are observed to have gouge zones that are on the order of millimeters to centimeters in width, in between that of mature faults and laboratory experiments (Ortlepp, 1997). Therefore, our estimate of D_c is consistent with this scaling. In fact, recent friction experiments using a 3-mm-thick gouge layer at shear speeds of up to 10 mm/sec report values of D_c of up to 1.8×10^{-4} m, agreeing well with our calculations (Mair and Marone, 1999).

Upper-Frequency Cutoff

The existence of a critical slip distance for nucleation of rupture makes a prediction about the corner frequency of the minimum earthquake. Average empirically determined values of *P*-wave speeds are 6,100 ± 60 m/sec. We can solve $f_0 = 2.01\ v_P/2\pi r_c$ (Madariaga, 1976) to determine the corner frequency of the minimum event. For $M_{\min} = 0.4$, we obtain ~100 Hz, but this is uncertain by 30%.

The reason for using estimates of source parameters to predict a corner frequency is that f_0 is an observable quantity in the seismic spectra; therefore, we have another means of testing our calculations of critical dimensions. In fact, the average *P*-wave corner frequency among all five mines for an $M = 0$ event is ~200 Hz, so these scaling relations are consistent with observations. Slip-weakening models predict that "f_{max}," the highest frequency recorded in the seismogram, is equal to the corner frequency of the minimum event because this is the patch size over which radiated energy is "smeared out."

We calculated spectra of the events that we reprocessed to test the model of $f_{\max}$ as a source property. As an example, we show the time-series accelerogram and spectrum recorded 487 m from an $M = 3.0$ event at Mponeng with $f_0 = 13.6$ Hz and $f_{\max} \sim 100$ Hz (Fig. 12). If $f_{\max}$ is a source property, it should be approximately equal for all events controlled by this source mechanism. We stacked several records of stations approximately 400 m distant from three events each to produce representative acceleration spectra for a large Type B event ($M = 2$), a small Type B event ($M = 0$), and a Type A event ($M = -0.4$). As the magnitude of Type B events decreases, $f_0 \rightarrow f_{\max} \sim 200$ Hz (Fig. 13; $f_{\max}$ is the vertical dashed line). The most important aspect of Figure 13 is that $f_{\max}$ appears to be constant at 150–200 Hz for Type B events, but we do not observe any $f_{\max}$ for the Type A events. This corroborates our hypothesis of the existence of a minimum earthquake at $M \sim 0$, where $f_0 \sim f_{\max}$, for Type B events.

Hanks (1982) observed a consistent high-frequency cutoff at 13 Hz in strong-motion recordings in southern California that he termed "f_{max}." Aki (1979, 1984, 1987) and Papageorgiou (1988) associated this with a source property and proposed $M_{\min} \sim 3$ for this region; however, studies by Hanks (1982, 1984) interpreted this $f_{\max}$ as the result of local site conditions instead. In this case, the alluvium or other non-hard-rock environment in which the sensor is placed causes rapid decay of spectral amplitudes at $f > f_{\max}$. In tectonic environments in which seismograms are recorded at fairly great hypocentral distances, $f_{\max}$ is influenced by attenuation along the ray path as well (Anderson and Hough 1984; Anderson 1986; Boore 1986). These sources of misinterpretation of $f_{\max}$ are not as problematic for this study because recordings only a few source radii away are not controlled by attenuation. For example, inelastic attenuation of the form $e^{-\pi fR/Qv_s}$ results in a distance-dependent $f_{\max} \sim$

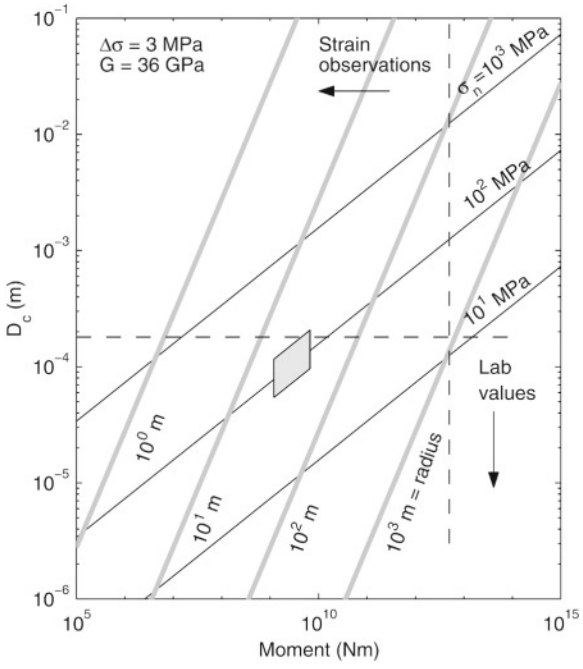

Figure 11. D_c vs. M_0 assuming $\Delta\sigma = 3$ MPa and $G = 36$ GPa, respectively. Black lines are lines of constant normal stress from 10 to 1,000 MPa. Gray lines are lines of constant source radius from 1 to 1,000 m. The shaded parallelogram denotes the range of moment magnitude of approximately 0–0.3 and a range of lithostatic normal stresses of 70–110 MPa, corresponding to the conditions for the critical patch size in the Far West Rand region. The critical patch size is on the order of 10 m and the critical slip distance is on the order of 10^{-4} m.

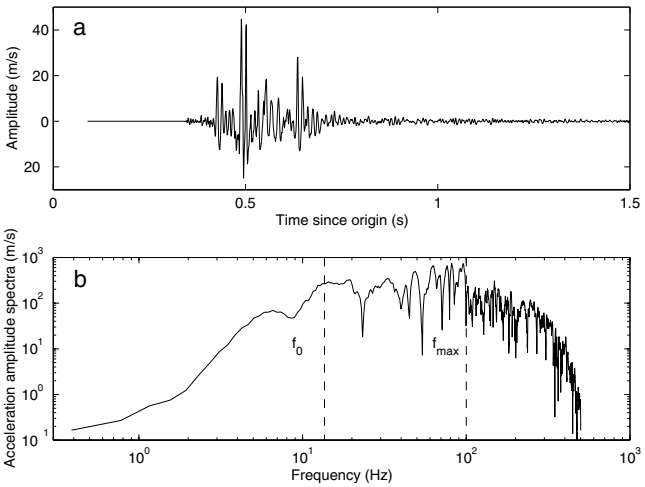

Figure 12. Vertical component accelerogram (a) and acceleration amplitude spectrum (b) for an $M = 3.0$ event in Mponeng on 02 February 2000 at 12:30:21 recorded 487 m from the source. In (a) the initial gap is the time difference between the origin of the event and the beginning of the triggered record. We calculated $f_0 = 13.6$ Hz for this event and estimated $f_{\max}$ at 100 Hz.

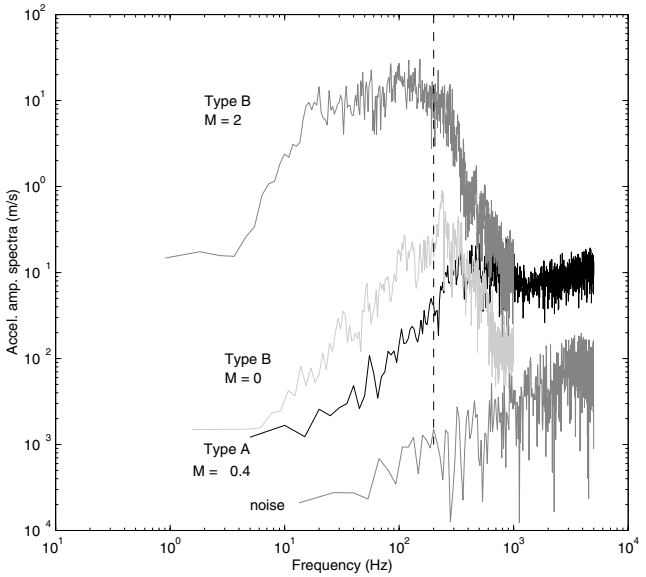

Figure 13. Stacked acceleration spectra from three events, each of $M \sim 2$, 0, and -0.4, along with a spectrum of noise. $f_{\max}$ is estimated at 150–200 Hz for the Type B stacks (vertical dashed line) but is not evident for the Type A stack. The noise spectrum was made by stacking the section of records between the trigger time and the P arrival. The source–receiver distance is approximately 400 m for all records.

$Qv_s/\pi R$. For $Q = 300$, $f_{\max} \sim 200$ Hz at 2 km from the source. At 400 m from the source, as in the records shown in Figure 13, the distance-dependent $f_{\max} \sim 900$ Hz. Also, the on-reef geophones are placed at depth in hard rock, so the site effects are expected to be small. Furthermore, we observed an $f_{\max}$ for Type B events, but not for Type A events, which are recorded by the same instruments at the same sites.

Implications of Apparent Stress Scaling

Many previous workers have observed apparent stress to increase with seismic moment within individual datasets (e.g., Kanamori *et al.*, 1993; Abercrombie, 1995; Mayeda and Walter, 1996; Izutani and Kanamori, 2001; and Prejean and Ellsworth, 2001). McGarr (1999) compared several of these datasets and concluded that there is a consistent upper limit to apparent stress across 17 orders of magnitude in seismic moment. He found that while each dataset's apparent stress scales with moment, it is unclear whether there is significant overall scaling behavior (McGarr, 1999). In addition, both the study of McGarr (1999) and recent work by Ide and Beroza (2001) suggest that the perceived scaling within each dataset is due to the underestimation of the energy of the smallest events or the omission of small events with high energies due to a finite recording bandwidth. Ide and Beroza (2001) applied a correction to account for the underestimated energy and compared the corrected datasets again. They concluded that while apparent stress values range over 3 orders of magnitude, there is no prominent scaling of apparent stress from 10^4 Nm to 10^{20} Nm.

We argue that there is indeed scaling of apparent stress with moment, yet the comparison of such a large range of event sizes has disguised the scaling for two reasons. The first is, as our characterization of the two different kinds of mining-induced seismicity shows, fracture- and friction-dominated events have different scaling properties. These events should be considered separately. The second is that data spanning the range of magnitudes in which the break between the two types of events occurs has been lacking from previous studies. The data in this study cover this gap and overlap with previous studies as well. Once all datasets are combined, scaling of apparent stress with moment is discernible for each of the two kinds of events.

We compared the apparent stresses and stress drops of the Type A events in this study with data from Canada's Underground Research Laboratory (Gibowicz *et al.*, 1991), the Strathcona Mine in Ontario, Canada (Urbancic *et al.*, 1993), and hydrofracturing events from the KTB borehole (Jost *et al.*, 1998). For the Gibowicz *et al.* (1991) data and the Jost *et al.* (1998) data, we used the corrected values of apparent stress from Ide and Beroza (2001). We also applied this correction to the Urbancic *et al.* (1993) data as well as to our own data. For our data, the correction was minimal (not visible on the scale of this plot), which we expected, since our corner frequencies were typically five to 10 times less than the Nyquist frequency. We binned each dataset in bins of 1 order of magnitude in moment and calculated the median value of σ_a and M_0 for each bin with its 95% confidence limit (open symbols in Fig. 14). We also found the mean and standard error of the mean by averaging the log of the data in each bin. These results were not significantly different from the medians, so we show only the medians for clarity. The apparent stress of these combined datasets decreases with seismic moment (Fig. 14).

In laboratory tests, the material strength of rock decreases with increasing sample size ($\text{size}^{-1/2}$) for samples on the order of 1 m. This scaling relationship is known as Petch's Law (Scholz, 1990). If we assume that apparent stress is a proxy for material strength for fracture-dominated events, then $\sigma_a \sim M_0^{-1/6}$, a slope that predicts the behavior of Type A events well (solid line in Fig. 14).

In contrast to the fracture-dominated Type A events, the Type B events are analogous to tectonic earthquakes in that their nucleation occurs under near-lithostatic normal stress and is therefore friction controlled. We compared the apparent stresses of our Type B data to studies of borehole recordings at Long Valley Caldera (Prejean and Ellsworth, 2001), and Cajon Pass (Abercrombie, 1995), as well as to the regionally recorded datasets of Mayeda and Walter (1996) and Kanamori *et al.* (1993). We used the corrected values of apparent stress from Ide and Beroza (2001) for the Kanamori *et al.* (1993) data and applied the correction to our Type B dataset. Again, we found no significant change for the Type B data. For the ensemble of friction-controlled

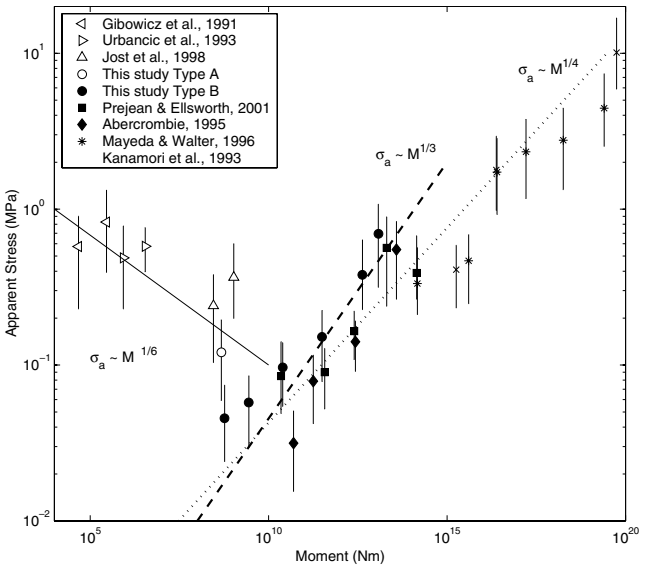

Figure 14. Medians with 95% confidence-error bars for σ_a vs. M_0 for the events in our study and several other studies. Each dataset is binned in order-of-magnitude units in moment. Open symbols represent fracture-dominated events, and the other symbols indicate friction-controlled datasets. An empirical scaling relation of $\sigma_a \sim M_0^{-1/6}$ for fracturing events is given by the solid line. Two relations for frictional events are given. The first ($\sigma_a \sim M_0^{-1/3}$) given by the dashed line fits only small, locally recorded events. In order for this scaling to fit large events, there must be a scale break and some saturation of apparent stress for large events. The second empirical relation for frictional events ($\sigma_a \sim M_0^{-1/4}$) given by the dotted line is intended to fit the entire range of these events.

events, σ_a increases with M_0 (Fig. 14). We found that for events of $M_0 < 10^{15}$ Nm, $\sigma_a \sim M_0^{1/3}$ (dashed line in Fig. 14). Models of enhanced velocity weakening due to melting have proposed that above $M_0 \sim 10^{15}$ Nm, apparent stress saturates at $\sim$ 2–4 MPa as stress drop becomes total (Kanamori and Heaton, 1998). Given the scatter in the regional datasets we examined here, the conclusion that apparent stress is constant above $M_0 \sim 10^{15}$ Nm cannot be ruled out. However, the range of data shown here does not require a scaling break and may perhaps be fit by a single empirical scaling of $\sigma_a \sim M_0^{1/4}$ (dotted line in Fig. 14). A physical explanation for this scaling is presently lacking, and further analysis of regional datasets that cover the bandwidth necessary to assess whether or not there is indeed a scaling break at $M_0 = 10^{15}$ Nm is beyond the scope of the present study. We note that the smallest values of apparent stress occur at the boundary between fracturing and frictional events, where the slip of frictional events is barely larger than the critical slip distance necessary for earthquake nucleation, so that the overall plot of apparent stress versus seismic moment has a V shape.

Proposed explanations of increasing apparent stress with seismic moment for friction-dominated events include the aforementioned hypothesis of enhanced velocity weakening of faults via melting during large events. In addition, scaling of rupture velocity with earthquake size, near-fault damage, or normal force fluctuations during rupture could cause large events to have higher radiated seismic energy and therefore higher apparent stress.

Conclusions

We have used deep South African gold mines as natural laboratories to observe fundamental aspects of rock failure, and we have quantified two distinct types of seismic events that occur in these mines. Previous workers in the field of mining-induced seismicity have discussed the idea of different classes of events (e.g., Gibowicz and Kijko, 1994), and more recently two populations have been separated spatially (Finnie, 1999b). Based on the properties of the seismicity we observed, we put forth a physical model for these two kinds of events. The Type A population is composed of small events, often related to blasts, whose nucleation occurs under low normal stress in competent rock and propagates as fractures with small process zones at the crack tip. These events have source-scaling relationships similar to other very small mining-induced and hydrofracturing events.

Type B events are characterized by process zones equal to the critical patch size over which the critical slip distance for seismic shear rupture is accommodated. The observation of the minimum earthquake size for the Type B events thus provides unique data on the scales of earthquake nucleation. We have calculated the critical dimensions of nucleation for the Type B events predicted by a slip-weakening model of fault friction based on source-scaling arguments and through observation of seismic spectra.

Observations of frequency–magnitude statistics of mine seismicity are a key part of this study. Frequency–magnitude distributions in which $b = 1$ are consistent with the theory of earthquake self similarity (Kanamori and Anderson, 1975; Rundle, 1989) in which stress drop is constant and the distribution of earthquake size follows a power law. We hypothesize that the decrease in frequency of the Type B events relative to a Gutenberg–Richter relationship below $M = 1$ is a departure from self similarity, indicative of a minimum event size for seismic rupture (Ida, 1973; Aki, 1987). The bandwidth of our dataset and the existence of the Type A events strengthen our conclusion that the cutoff in magnitude observable for Type B events is genuine. Our calculations of the critical dimensions of earthquake nucleation agree with extrapolations from laboratory results and tectonic datasets.

We interpret our observation of an $f_{\max}$ in the acceleration spectra as further evidence of a minimum earthquake for Type B events. In so doing, we follow the model proposed by Papageorgiou and Aki (1983a,b), in which the maximum frequency recorded in the acceleration power spectra of the largest earthquakes in a region should be approximately equal to the corner frequency of the smallest earthquake

in the region. Previous workers have observed an f_{max} in mining-induced seismicity data. Cichowicz *et al.* (1990) proposed that for very small events ahead of a stope face, $f_{max} \sim 5$ kHz, and Young *et al.* (1989) observed $f_{max} \sim 3$ kHz. These values are an order of magnitude higher than our observations for Type B events, so it is likely that the events in these two previous studies were Type A events. Although we did not observe an f_{max} for Type A events, we also do not have the bandwidth in this study to make a reasonable comparison with the previous studies. We do note that high f_{max} (or none) for very small events is consistent with our physical model of Type A events as having a process zone at the grain-scale level.

Our assumption that Type B events are analogous to tectonic earthquakes implies that the calculations of the critical dimensions of rupture nucleation for mining seismicity extend to that for tectonic events. An interesting result of these calculations from the point of view of earthquake physics is that observing the nucleation of an event with a radius on the order of 10 m and with a critical slip distance on the order of 10^{-4} m will be extremely difficult with present surface-based seismographic networks. In fact, this size is approximately the smallest well-recorded source dimension at the Parkfield network (Nadeau and Johnson, 1998).

Although there is uncertainty in our estimates of how earthquake sources scale at small magnitudes, fundamental processes such as end-zone size, critical patch size, and displacement needed to nucleate seismic slip have not been observed at this level before. Approaching the study of these processes simultaneously from the fields of earthquake seismology, laboratory friction experiments, and mining seismology will aid in bridging the scale gap between observations and theory.

Acknowledgments

We wish to thank AngloGold, Ltd., for access to their data and for the considerable aid and expertise provided by the many AngloGold, Ltd., employees who facilitated visits underground, made data available, and took time to discuss observations, particularly Dragan Amidzic. We are grateful for technical support and from those at ISS International, Ltd., especially Alex Mendecki and Gerrie Van Aswegen. We thank Stephanie Prejean, Rachel Abercrombie, and Satoshi Ide for making their data available to us. Discussions with Steve Spottiswoode, Lindsay Andersen, and Ewan Sellers of CSIR Miningtek were valuable, as were critiques of this manuscript by George Gibowicz, Art McGarr, and an anonymous reviewer. This project was sponsored by DSWA contract number DSWA01-98-C-0158.

References

Abercrombie, R. E. (1995). Earthquake locations using single-station deep borehole recordings: implications for microseismicity on the San Andreas fault in southern California, *J. Geophys. Res.* **100,** 24,003–24,014.

Aki, K. (1967). Scaling law of seismic spectrum, *J. Geophys. Res.* **72,** 1217–1231.

Aki, K. (1979). Characterization of barriers on an earthquake fault, *J. Geophys. Res.* **84,** 6140–6148.

Aki, K. (1984). Asperities, barriers, characteristic earthquakes and strong motion prediction, *J. Geophys. Res.* **89,** 5867–5872.

Aki, K. (1987). Magnitude-frequency relation for small earthquakes: a clue to the origin of f_{max} of large earthquakes, *J. Geophys. Res.* **92,** 1349–1355.

Andersen, L. M. (1999). A relative moment tensor inversion technique applied to seismicity induced by mining, *Master's Thesis*, University of the Witwatersrand, Johannesburg, Republic of South Africa.

Anderson, J. G. (1986). Implication of attenuation for studies of the earthquake source, in *Earthquake Source Mechanics*, S. Das, J. Boatwright, and C. H. Scholz (Editors), Vol. 6, American Geophysical Monograph 37, 311–318.

Anderson, J. G., and S. E. Hough (1984). A model for the shape of the Fourier amplitude spectrum of acceleration at high frequencies, *Bull. Seism. Soc. Am.* **74,** 1969–1993.

Andrews, D. J. (1976a). Rupture propagation with finite stress in antiplane strain, *J. Geophys. Res.* **81,** 3575–3582.

Andrews, D. J. (1976b). Rupture velocity of plane strain shear cracks, *J. Geophys. Res.* **81,** 5679–5687.

Andrews, D. J. (1986). Objective determination of source parameters and similarity of earthquakes of different size, in *Earthquake Source Mechanics*, S. Das, J. Boatwright, and C. H. Scholz (Editors), Vol. 6, American Geophysical Monograph 37, 259–267.

Baker, C., and R. P. Young (1997). Evidence for extensile crack initiation in point source time-dependent moment tensor solutions, *Bull. Seism. Soc. Am.* **87,** 1442–1453.

Barenblatt, G. S. (1959). Concerning equilibrium cracks forming during brittle fracture: the stability of isolated cracks, relationships with energetic theories, *Appl. Math. Mech.* **23,** 1273–1282.

Biegel, R. L., C. G. Sammis, and J. H. Dieterich (1989). The frictional properties of a simulated gouge having a fractal particle distribution, *J. Struct. Geol.* **11,** 827–846.

Boore, D. M. (1986). The effect of finite bandwidth of seismic scaling relationships, in *Earthquake Source Mechanics*, S. Das, J. Boatwright, and C. H. Scholz (Editors), Vol. 6, American Geophysical Monograph 37, 275–283.

Brune, J. N. (1970). Tectonic stress and the spectra of seismic shear waves from earthquakes, *J. Geophys. Res.* **75,** 4997–5009; Correction, (1974) *J. Geophys. Res.* **76,** 5002.

Cichowicz, A., R. W. E. Green, A. van Zyl Brink, P. Grobler, and P. I. Mountfort (1990). The space and time variation of micro-event parameters occurring in front of an active stope, in *Rockbursts and Seismicity in Mines*, C. Fairhurst (Editor), Vol. 2, 171–175.

Cook, N. G. W. (1963). The seismic location of rockbursts, in Proceedings of the 5th Symposium on Rock Mechanics, Pergamon, Oxford, 493–516.

Dieterich, J. H. (1978). Time-dependent friction and the mechanics of stick-slip, *Pure Appl. Geophys.* **116,** 790–805.

Dieterich, J. H. (1979). Modeling of rock friction, 1: experimental results and constitutive equations, *J. Geophys. Res.* **84,** 2161–2168.

Dieterich, J. H. (1986). A model for the nucleation of earthquake slip, in *Earthquake Source Mechanics*, S. Das, J. Boatwright, and C. H. Scholz (Editors), Vol. 6, American Geophysical Monograph 37, 37–47.

Feignier, B., and R. P. Young (1992). Moment tensor inversion of induced microseismic events: evidence of non-shear failures in the $-4 < m < -2$ moment magnitude range, *Geophys. Res. Lett.* **19,** 1503–1506.

Finnie, G. J. (1999a). Some statistical aspects of mining induced seismic events, in *2nd Southern African Rock Engineering Symposium*, T. O. Hagan (Editor), Johannesburg, South Africa.

Finnie, G. J. (1999b). Using neural networks to discriminate between genuine and spurious seismic events in mines, *Pure Appl. Geophys.* **154**, 41–56.

Gibowicz, S. J. (1990). The mechanism of seismic events induced by mining—a review, in *Rockbursts and Seismicity in Mines*, C. Fairhurst (Editor), Balkema, Rotterdam, 3–28.

Gibowicz, S. J. (1997). An anatomy of a seismic sequence in a deep gold mine, *Pure Appl. Geophys.* **150,** 393–414.

Gibowicz, S. J., and A. Kijko (1994). *An Introduction to Mining Seismology*, Academic New York.

Gibowicz, S. J., R. P. Young, S. Talebi, and D. J. Rawlence (1991). Source parameters of seismic events at the Underground Research Laboratory in Manitoba, Canada: scaling relations for events with moment magnitude smaller than −2, *Bull. Seism. Soc. Am.* **81,** 1157–1182.

Hanks, T. C. (1982). $f_{\max}$, *Bull. Seism. Soc. Am.* **72,** 1867–1879.

Hanks, T. C. (1984). a_{rms} and seismic source studies, in *Proceedings of the 1st International Congress on Rockbursts and Seismicity in Mines*, N. C. Gay and E. H. Wainwright (Editors), Johannesburg, South African Institute of Mining and Metallurgy, 39–44.

Hanks, T. C., and H. Kanamori (1979). A moment magnitude scale, *J. Geophys. Res.* **84,** 2348–2350.

Ida, Y. (1972). Cohesive force across the tip of a longitudinal shear crack and Griffith's specific surface energy, *J. Geophys. Res.* **77,** 3796–3805.

Ida, Y. (1973). The maximum acceleration of seismic ground motion, *Bull. Seism. Soc. Am.* **63,** 959–968.

Ide, S., and G. C. Beroza (2001). Does apparent stress vary with earthquake size?, *Geophys. Res. Lett.* **28,** 3349–3352.

Izutani, Y., and H. Kanamori (2001). Scale-dependence of seismic energy-to-moment ratio for strike-slip earthquakes in Japan, *Geophys. Res. Lett.* **28,** 4007–4010.

Johnston, J. C. (1988). A survey of mining associated rockbursts, *Master's Thesis*, Massachusetts Institute of Technology.

Johnston, J. C., and M. H. Einstein (1990). A survey of mining associated seismicity, in *Rockbursts and Seismicity in Mines*, C. Fairhurst (Editor), Balkema, Rotterdam, 121–125.

Jost, M. L., T. Büβelberg, Ö. Jost, and H. P. Harjes (1998). Source parameters of injection-induced microearthquakes at 9 km depth at the KTB deep drilling site, Germany, *Bull. Seism. Soc. Am.* **88,** 815–832.

Joughin, N. C., and A. J. Jager (1983). Fracture of rock at stope faces in South African gold mines, in *Rockbursts: Prediction and Control*, L. Richards (Editor), Institute of Mining and Metallurgy, London, 53–66.

Kanamori, H., and D. Anderson (1975). Theoretical basis of some empirical relations in seismology, *Bull. Seism. Soc. Am.* **65,** 1073–1095.

Kanamori, H., and T. H. Heaton (1998). Constraints on earthquake inferred from radiated energy, *EOS* **79,** F. 610.

Kanamori, H., J. Mori, E. Hauksson, T. H. Heaton, L. K. Hutton, and L. M. Jones (1993). Determination of earthquake energy release and m_l using TERRAscope, *Bull. Seism. Soc. Am.* **83,** 330–346.

Kijko, A., B. Drzezla, and T. Stankiewicz (1987). Bimodal character of the distribution of extreme seismic events in Polish mines, *Acta Geophys. Pol.* **35,** 159–168.

Madariaga, R. (1976). Dynamics of an expanding circular fault, *Bull. Seism. Soc. Am.* **66,** 639–666.

Mair, K., and C. Marone (1999). Friction of simulated fault gouge for a wide range of velocities, *J. Geophys. Res.* **104,** 28,899–28,914.

Marone, C. (1998). Laboratory-derived friction laws and their application to seismic faulting, *Annu. Rev. Earth Planet. Sci.* **26,** 643–696.

Marone, C., and B. Kilgore (1993). Scaling of the critical slip distance for seismic faulting with shear strain in fault zones, *Nature* **362,** 618–621.

Mayeda, K., and W. R. Walter (1996). Moment, energy, stress drop, and source spectra of western United States earthquakes from regional coda envelopes, *J. Geophys. Res.* **101,** 11,195–11,208.

McGarr, A. (1971). Violent deformation of rock near deep-level tabular excavations-seismic events, *Bull. Seism. Soc. Am.* **61,** 1453–1466.

McGarr, A. (1984a). Scaling of ground motion parameters, state of stress, and focal depth, *J. Geophys. Res.* **89,** 6969–6979.

McGarr, A. (1984b). Some applications of seismic source mechanism studies to assessing underground hazard, in *Proceedings of the 1st International Congress on Rockbursts and Seismicity in Mines, Johannesburg*, N. C. Gay and E. H. Wainwright (Editors) South African Institute of Mining and Metallurgy, Johannesburg, 199–208.

McGarr, A. (1992a). An implosive component in the seismic moment tensor of a mining-induced tremor, *Geophys. Res. Lett.* **19,** 1579–1582.

McGarr, A. (1992b). Moment tensors of ten Witwatersrand mine tremors, *Pure Appl. Geophys.* **139,** 781–800.

McGarr, A. (1999). On relating apparent stress to the stress causing earthquake fault slip, *J. Geophys. Res.* **104,** 3003–3011.

Mendecki, A. J. (Editor) (1997). *Seismic Monitoring in Mines*, Chapman & Hall, London.

Nadeau, R. M., and L. R. Johnson (1998). Seismological studies at Parkfield VI: moment release rates and estimates of source parameters for small repeating earthquakes, *Bull. Seism. Soc. Am.* **88,** 790–814.

Nadeau, R. M., and T. V. McEvilly (1999). Fault slip rates at depth from recurrence intervals of repeating microearthquakes, *Science* **285,** 718–721.

Ortlepp, W. D. (1997). *Rock Fracture and Rockbursts: An Illustrative Study*, South African Institute of Mining and Metallurgy, Johannesburg.

Palmer, A. C., and J. R. Rice (1973). The growth of slip surfaces in the progressive failure of over-consolidated clay, *Proc. R. Soc. London A* **332,** 527–548.

Papageorgiou, A., and K. Aki (1983a). A specific barrier model for the quantitative description of inhomogeneous faulting and the prediction of strong ground motion, I: description of the model, *Bull. Seism. Soc. Am.* **73,** 693–722.

Papageorgiou, A., and K. Aki (1983b). A specific barrier model for the quantitative description of inhomogeneous faulting and the prediction of strong ground motion, II: applications of the model, *Bull. Seism. Soc. Am.* **73,** 953–978.

Papageorgiou, A. S. (1988). On two characteristic frequencies of acceleration spectra: patch corner frequency and $f_{\max}$, *Bull. Seism. Soc. Am.* **78,** 509–529.

Prejean, S. G., and W. L. Ellsworth (2001). Observations of earthquake source parameters at 2 km depth in the Long Valley caldera, eastern California, *Bull. Seism. Soc. Am.* **91,** 165–177.

Prugger, A. F., and D. J. Gendzwill (1990). Results of microseismic monitoring at the Cory mine, 1981–1984, in *Rockbursts and Seismicity in Mines*, C. Fairhurst (Editor), Rotterdam, Balkema, 215–219.

Rubin, A. M., D. Gillard, and J.-L. Got (1999). Streaks of microearthquakes along creeping faults, *Nature* **400,** 635–641.

Ruina, A. (1983). Slip instability and state variable friction laws, *J. Geophys. Res.* **88,** 10,359–10,370.

Rundle, J. B. (1989). Derivation of the complete Gutenberg–Richter magnitude–frequency relation using the principle of scale invariance, *J. Geophys. Res.* **94,** 12,337–12,342.

Rydelek, P. A., and I. S. Sacks (1989). Testing the completeness of earthquake catalogues and the hypothesis of self-similarity, *Nature* **337,** 251–253.

Sammis, C. G., and S. J. Steacy (1994). The micromechanics of friction in a granular layer, *Pure Appl. Geophys.* **142,** 777–794.

Scholz, C. H. (1988). The critical slip distance for seismic faulting, *Nature* **336,** 761–763.

Scholz, C. H. (1990). *The Mechanics of Earthquakes and Faulting*, Cambridge Press, New York, 439 pp.

Spottiswoode, S. M., and A. McGarr (1975). Source parameters of tremors in a deep-level gold mine, *Bull. Seism. Soc. Am.* **65,** 93–112.

Talebi, S., and R. P. Young (1990). Characterizing microseismicity associated with stope development, in *Rockbursts and Seismicity in Mines*, C. Fairhurst (Editor), Balkema, Rotterdam, 189–194.

Taylor, D. W. A., J. A. Snoke, I. S. Sacks, and T. Takanami (1990). Nonlinear frequency–magnitude relationships for the Hokkaido Corner, Japan, *Bull. Seism. Soc. Am.* **80,** 340–353.

Trifu, C.-I., and M. Radulian (1991). Frequency-magnitude distribution of earthquakes in Vrancea: relevance for a discrete model, *J. Geophys. Res.* **96,** 4301–4311.

Trifu, C.-I., T. I. Urbancic, and R. P. Young (1993). Non-similar frequency-magnitude distribution for $m < 1$ seismicity, *Geophys. Res. Lett.* **20,** 427–430.

Urbancic, T. I., C.-I. Trifu, and R. P. Young (1993). Microseismicity derived fault-planes and their relationship to focal mechanism, stress inversion, and geologic data, *Geophys. Res. Lett.* **20,** 2475–2478.

Wong, I. G., and A. McGarr (1990). Implosional failure in mining-induced seismicity: a critical review, in *Rockbursts and Seismicity in Mines*, C. Fairhurst (Editor), Balkema, Rotterdam, 45–51.

Young, R. P., S. Talebi, D. A. Hutchins, and T. I. Urbancic (1989). Analysis of mining-induced microseismic events at Strathcona Mine, Sudbury, Canada, *Pure Appl. Geophys.* **129,** 455–474.

Dept. of Earth Sciences
University of Southern California
Los Angeles, California
(T.H.J.)

Department of Geosciences
Pennsylvania State University
University Park, Pennsylvania
(E.R.)

Manuscript received 2 August 2000.